HAL open science

Synthesis and characterization of analogues of glycine-betaine ionic liquids and their use in the formation of aqueous biphasic systems

Matheus Pereira, Sónia Pedro, Joana Gomes, Tania E. Sintra, Sónia P.M. Ventura, João A.P. Coutinho, Mara G. Freire, Aminou Mohamadou

To cite this version:

Matheus Pereira, Sónia Pedro, Joana Gomes, Tania E. Sintra, Sónia P.M. Ventura, et al.. Synthesis and characterization of analogues of glycine-betaine ionic liquids and their use in the formation of aqueous biphasic systems. Fluid Phase Equilibria, 2019, 494, pp.239-245. 10.1016/j.fluid.2019.05.001 . hal-02429718

HAL Id: hal-02429718

https://hal.univ-reims.fr/hal-02429718

Submitted on 25 Oct 2021

HAL is a multi-disciplinary open access archive for the deposit and dissemination of scientific research documents, whether they are published or not. The documents may come from teaching and research institutions in France or abroad, or from public or private research centers.

L'archive ouverte pluridisciplinaire **HAL**, est destinée au dépôt et à la diffusion de documents scientifiques de niveau recherche, publiés ou non, émanant des établissements d'enseignement et de recherche français ou étrangers, des laboratoires publics ou privés.

Distributed under a Creative Commons Attribution - NonCommercial 4.0 International License

Version of Record: https://www.sciencedirect.com/science/article/pii/S0378381219302031
Manuscript_f16395fedf4c1bebabb6fc8f712d52de

Synthesis and characterization of analogues of glycine-betaine ionic liquids and their use in the formation of aqueous biphasic systems

Matheus M. Pereira[1], Sónia N. Pedro[1], Joana Gomes[1], Tânia E. Sintra[1], Sónia P. M. Ventura[1], João A. P. Coutinho[1], Mara G. Freire[1], Aminou Mohamadou[2]*

[1]CICECO – Aveiro Institute of Materials, Department of Chemistry, University of Aveiro, Campus Universitário de Santiago, 3810-193 Aveiro, Portugal

[2]Institut de Chimie Moléculaire de Reims (ICMR), UMR CNRS 7312, Université de Reims Champagne-Ardenne, Moulin de la Housse, BP 1039 – 51687 Reims cedex 2, France.

* Corresponding author: Tel: +33 (0)32691 3334; Fax: +33 (0)32691 3243
E-Mail : aminou.mohamadou@univ-reims.fr (A. Mohamadou)

© 2019 published by Elsevier. This manuscript is made available under the CC BY NC user license
https://creativecommons.org/licenses/by-nc/4.0/

Abstract

A series of novel analogues of glycine-betaine ionic liquids (AGB-ILs), viz. 1-(4-ethoxy-4-oxobutyl)-1-methylpyrrolidin-1-ium, N,N,N-tri(*n*-butyl)(4-ethoxy-4-oxobutyl)-1-phosphonium and N,N,N-trialkyl(4-ethoxy-4-oxobutyl)-1-aminium cations with ethyl, *n*-propyl and *n*-butyl alkyl chains, combined with the bromide anion, have been synthesized and characterized. Their synthesis and characterization by spectroscopic methods and elemental analysis is here reported. These ILs were further characterized in what concerns their thermal properties and ecotoxicity against *Allvibrio fischeri*, and compared with the commercial tetra(*n*-butyl)ammonium and tetra(*n*-butyl)phosphonium bromide. The novel AGB-ILs described in this work have low melting points, below 100 °C, display high degradation temperatures (180-310 °C), and low toxicity as shown by being harmless or practically harmless towards the marine bacteria *Allvibrio fischeri*. Finally, the ability of the synthesized AGB-ILs to form aqueous biphasic systems with potassium citrate/citric acid (at pH 7) was evaluated, and the respective ternary phase diagrams were determined. It is shown that the increase of the cation alkyl chain length facilitates the creation of ABS, and that phosphonium-based ILs present a slightly better separation performance in presence of aqueous solutions of the citrate-based salt.

Key words: Ionic liquids, analogues of glycine-betaine, thermal properties, ecotoxicity, *Allvibrio fischeri*, aqueous biphasic systems, phase diagram.

1. Introduction

In order to replace volatile organic solvents, which may be harmful to both the process operators and the environment [1], many researchers have focused on the development of "greener solvents" [2]. Amongst these solvents, aprotic ionic liquids (ILs) are an interesting class of fluids since, if properly designed, they display a negligible vapour pressure at ambient conditions, non-flammability, high chemical and thermal stabilities, and unique solvation capabilities. As a result of these features, they have attracted attention as solvents for chemical and electrochemical reactions, biphasic catalysis, chemical syntheses, separation processes, among others [3-6]. Nevertheless, some ILs may display some toxicity and cause biodegradability concerns [7, 8]. Therefore, the design of more environmentally benign ILs has been a hot topic over the past years [9]. To obtain "greener" ILs, the starting materials should be non-toxic and renewable, and their synthesis environmentally-friendly [10]. The synthesis of ILs from renewable raw materials is more beneficial and attractive compared to the use of compounds derived from fossil feedstocks. In recent years, several bio-based ILs with biocompatible character have been synthesized and characterized, receiving considerable attention for distinct applications [11, 12]. Cholinium based-ILs emerged in several reports as biocompatible alternatives over the well-known imidazolium-based counterparts on the dissolution of biomass, CO_2 absorption processes or biomaterials development [13-15]. More recently, amino-acid- and carbohydrate-based ILs have been proposed to improve the biocompatible properties of ILs. The first have been tested in the pretreatment of lignocellulosic materials and as catalysts in organic synthesis [16-19], while the later have recently been proposed as novel chiral solvents [20, 21].

Previously, we reported the synthesis and characterization of ILs wherein the cation is either an alkyl ester glycine-betaine (GB) [22] or an analogue of glycine-betaine (AGB) [23], in which the ammonium cation comprises three alkyl groups and an ethyl acetate group. Hydrophobic GB-ILs have been applied in liquid-liquid extraction of pesticides [24], while AGB-ILs were employed in the extraction of metals from aqueous solutions [25-27]. On the other hand, hydrophilic (water-miscible) AGB-ILs have been used in the extraction of value-added compounds from biomass [28]. The cytotoxicity of these ILs aqueous solutions containing the biomass extracts was assessed in a macrophage cell line, as well as their anti-inflammatory potential via reduction of lipopolysaccharide-induced cellular oxidative stress, showing that the IL aqueous solutions enriched in the biomass extracts display higher antioxidant and anti-inflammatory effects than the recovered solid extracts, and that these solutions may be used in nutraceutical and cosmetic applications [28].

Glycine-betaine, which is a zwitterionic acetate group bearing a quaternary tri(methyl)ammonium, can be found in sugar beet molasses (up to 27 wt%) after the extraction of saccharose [29]. These organic osmolytes are recognized by their accumulation in a wide variety of plants in response against environmental stress. They have positive effects on enzyme and membrane

integrity along with adaptive roles in mediating osmotic adjustment in plants growing under stress conditions [30, 31]. Furthermore, glycine-betaine and their derivatives are currently used as food supplements [32], as well as in cosmetic lotions and formulations [33]. Given the benefits and "green" credentials associated to glycine-betaine, we hereby report on the synthesis and characterization of 5 new bromide-based AGB-ILs, in which the cation carries an ethyl ester butyrate and three alkyl groups. Two commercial ILs, namely tetrabutylammonium bromide and tetrabutylphosphonium bromide, were also investigated for comparison purposes. The AGB-ILs synthesis and characterization are reported, and their thermal properties, such as melting point, glass transition temperature and decomposition temperature, were determined. The ecotoxicity of the synthesized AGB-ILs towards *Allvibrio fischeri* was assessed using the Microtox® acute toxicity test [34, 35]. Finally, while envisaging their application in separation processes, their ability to create aqueous biphasic systems (ABS) in presence of potassium citrate was investigated.

2. Experimental Section

2.1. Materials

All used chemicals are described in Table 1, which comprises the CAS number, molecular weigth, purity and supplier.

Table 1

Name, CAS number, molecular weigth, purity and supplier of the used chemicals.

Reagents	CAS number	Molecular weigth	Purity (%)	Supplier
N-methylpyrrolidine	121-44-8	85.15	≥ 97	Sigma Aldrich
triethylamine	121-44-8	101.19	> 99	Fischer Scientific
tri(*n*-propyl)amine	102-69-2	143.27	≥ 98	Sigma Aldrich
tri(*n*-butyl)amine	102-82-9	185.35	≥ 98	Fischer Scientific
4-bromobutyric acid ethyl ester	2969-81-5	195.05	≥ 97	Sigma Aldrich
tripotassium citrate monohydrate	6100-05-6	324.42	≥ 99	Fischer Scientific
citric acid monohydrate·H_2O	5949-29-1	210.14	100	Sigma Aldrich
tetrabutylammonium bromide	1643-19-2	322.37	> 97	Fluka
tetrabutylphosphonium bromide	3115-68-2	339.33	> 98	Sigma Aldrich

2.2. Synthesis of AGB-ILs

2.2.1. 1-(4-ethoxy-4-oxobutyl)-1-methylpyrrolidin-1-ium bromide ([MepyrNC$_4$]Br · H$_2$O)

A solution of 4-bromobutyrate acid ethyl ester (42.9 g, 0.22 mol) in ethyl acetate (100 mL) was added to a solution of N-methylpyrrolidine (29.8 g, 0.35 mol) in 110 mL of ethyl acetate. The mixture was stirred at room temperature for 24 days. The precipitate produced during the reaction was filtered, and washed twice with ethyl acetate and then with ethyl ether, and dried under vacuum. Yield (54.5 g, 83%). Elemental analysis: Found: C, 44.40; H, 7.80; N, 4.70%. Calculated for $C_{11}H_{24}BrNO_3$ (MW = 298.22 g·mol^{-1}): C, 44.30; H, 8.11; N, 4.70%. ^{1}H NMR, δ/ppm (300 MHz, DMSO-d_6): 1.20 [3 H, t, CH$_3$(β)]; 2.01 [2 H, m, CH$_2$(2)]; 2.08 (2 H, s, CH$_3$(c)]; 2.41 [2 H, t, CH$_2$(3)]; 3.38 [2 H, m, CH$_2$(b)]; 3.56 (6 H, m, CH$_2$(a+1)]; 4.09 (2 H, q, CH$_2$(α)]. ^{13}C NMR, δ/ppm (75.47 MHz, DMSO-d_6): 11.2 [CH$_3$(β)]; 14.8 [CH$_3$(c)]; 19.1 [CH$_2$(2)]; 21.7 [CH$_2$(3)]; 23.0 [CH$_2$(1)]; 31.3 [CH$_2$(b)]; 56.9 3 [CH$_2$(a)]; 60.5 [CH$_2$(α)]; 172.5 [C=O(4)]. ESI-MS, m/z Found (Calculated): 200.16 (200.30) [$C_{11}H_{22}NO_2^+$]; 115.07 (115.15) [$C_6H_{11}O_2^+$]. IR (ν/cm^{-1}): 3390 (ν_{O-H}); 2955, 2870 (ν_{C-H}); 1720 ($\nu_{C=O}$); 1286 (ν_{C-N}).

2.2.2. N,N,N-tri(*n*-alkyl)(4-ethoxy-4-oxobutyl)-1-aminium bromide

Tri(ethyl)[4-ethoxy-4-oxobutyl]ammonium bromide and Tri(*n*-propyl)[4-ethoxy-4-oxobutyl]ammonium bromide were synthesized as described for (N-methylpyrrolidyl-4-ethoxy-4-oxobutyl)ammonium bromide using tri(ethyl)amine (35.4 g, 0.35 mol) and tri(*n*-propyl)amine (50.1 g, 0.35 mol), respectively.

2.2.2.1. N,N,N-tri(ethyl)(4-ethoxy-4-oxobutyl)-1-aminium bromide ([Et$_3$NC$_4$]Br · 0.2 H$_2$O)

Yield (52.8 g, 80%). Elemental analysis: Found: C, 48.00; H, 8.90; N, 4.50%. Calculated for $C_{12}H_{24.4}BrNO_{2.2}$ (MW = 299.85 g·mol^{-1}): C, 48.07; H, 8.87; N, 4.67%. ^{1}H NMR, δ/ppm (300 MHz, DMSO-d_6): 1.19 [12 H, m, CH$_3$(β+b)]; 1.88 [2 H, m, CH$_2$(2)]; 2.45 [2 H, t, H$_2$(3)]; 3.15 [2 H, t, CH$_2$(1)]; 3.24 [6H, q, CH$_2$(a)]; 4.08 [2 H, q, CH$_2$(α)]. ^{13}C NMR, δ/ppm (75.47 MHz, DMSO-d_6): δ 14.1 [CH$_3$(b)]; 19.6 [CH$_3$(β)]; 23.5 [CH$_2$(2)]; 58.0 [CH$_2$(a)], 60.7 [CH$_2$(1)]; 62.7 [CH$_2$(α)]; 172.4 [C=O(4)]. ESI-MS, m/z Found (Calculated): 216.1_ (216.34) [$C_{12}H_{26}NO_2^+$]; 115.08 (115.15) [$C_6H_{11}O_2^+$] IR (ν/cm^{-1}): 3400 (ν_{O-H}); 2950, 2865 (ν_{C-H}); 1725 ($\nu_{C=O}$); 1280 (ν_{C-N}).

2.2.2.2. N,N,N-tri(*n*-propyl)(4-ethoxy-4-oxobutyl)-1-aminium bromide ([Pr$_3$NC$_4$]Br · 0.7 H$_2$O)

Yield (62.5 g, 81%). Elemental analysis: Found: C, 51.50; H, 9.60; N, 4.20%. Calculated for $C_{15}H_{33.4}BrNO_{2.7}$ (MW = 350.94 g·mol^{-1}): C, 51.34; H, 9.59; N, 3.99%. ^{1}H NMR, δ/ppm (300 MHz, DMSO-d6): 0.90 [9 H, t, CH$_3$(c)]; 1.20 [3 H, t, CH$_3$(β)]; 1.65 [6 H, m, CH$_2$(b)]; 1.81 [2 H, m, CH$_2$(2)]; 2.43 [2 H, t, CH$_2$(3)]; 3.20 (8 H, m, CH$_2$(a+1)]; 4.08 (2 H, q, CH$_2$(α)]. 13C NMR, δ/ppm (75.47 MHz,

DMSO-d6): 11.1 [CH_3(c)]; 14.4 [CH_3(β)]; 15.2 [CH_2(b)]; 16.8 [CH_2(2)]; 30.1 [CH_2(3)]; 59.7 [CH_2(a+1)]; 60.7 [CH_2(α)]; 172.4 [C=O(4)]. ESI-MS, m/z Found (Calculated): 258.24 (258.42) [$C_{15}H_{32}NO_2^+$]; 115,08 (115,15) [$C_6H_{11}O_2^+$] IR (ν/cm^{-1}): 3450 (ν_{O-H}); 2957, 2866 (ν_{C-H}); 1728 ($\nu_{C=O}$); 1285 (ν_{C-N}).

2.2.3. N,N,N-tri(*n*-butyl)(4-ethoxy-4-oxobutyl)-1-aminium bromide ([Bu_3NC_4]Br)

To tri(*n*-butyl)amine (68.9 g, 0.35 mol) in 110 mL of ethyl acetate, it was added (42.9 g, 0.22 mol) 4-bromobutyrate acid in 100 mL of ethyl ester, under stirring. The mixture was refluxed for 48h and then stirred at room temperature for 2h. The solution separates into two phases, and the bottom phase corresponding to the brownish oil was recovered, and washed three times with 100 mL of ethyl acetate, and then kept in the freezer for 48 h. The white product, which crystallized after 48 hours, was successively washed with ethyl acetate and diethyl ether, and then dried under vacuum. Yield (71.1 g, 85%). Elemental analysis: Found: C, 57.04; H, 9.90; N, 3.50%. Calculated for $C_{18}H_{38}BrNO_2$ (MW = 380.41 g·mol^{-1}): C, 56.83; H, 10.07; N, 3.68%. ^{1}H NMR (300 MHz, DMSO-d_6): 0.94 [9 H, t, CH_3(d)]; 1.21 [3 H, t, CH_3(β)]; 1.37 [6 H, m, CH_2(c)]; 1.64 [6 H, m, CH_2(b)]; 1.89 [2 H, m, CH_2(2)]; 2.43 [2 H, t, CH_2(3)]; 3.21 [8 H, m, CH_2(a+1)]; 4.09 [2 H, q, CH_2(α)]. ^{13}C NMR, δ/ppm (75.47 MHz, DMSO-d_6): 14.1 [CH_3(d)]; 19.6 [CH_3(β)], 23.5 [CH_3(c)]; 33.1 [CH_2(2)]; 56.8 [CH_2(b)]; 58.0 [CH_2(3)]; 60.7 [CH_2(1+a)]; 62.7 [CH_2(α)]; 172.2 [C=O(4)]. ESI-MS, m/z Found (Calculated): 300.27 (300.50) [$C_{18}H_{38}NO_2^+$]; 115.08 (115.15) [$C_6H_{11}O_2^+$] IR (ν/cm^{-1}): 2960, 2872 (ν_{C-H}); 1728 ($\nu_{C=O}$); 1283 (ν_{C-N}).

2.2.4. Tri(*n*-butyl)(4-ethoxy-4-oxobutyl)-1-phosphonium bromide ([Bu_3PC_4]Br)

Tri(*n*-butyl)[4-ethoxy-4-oxobutyl]phosphonium bromide was synthesized as described for N,N,N-tri(*n*-butyl)(4-ethoxy-4-oxobutyl)-1-aminium bromide using tri(*n*-butyl)phosphine (65.2 g, 0.35 mol) as amine. Yield (73.4 g, 84%). Elemental analysis: Found: C, 54.36; H, 9.85%. Calculated for $C_{18}H_{38}BrPO_2$ (MW = 397.37 g·mol^{-1}): C, 54.42; H, 9.58%. ^{1}H NMR (300 MHz, DMSO-d_6): 0.90 [9H, t, CH_3(d)]; 1.24 [3H, t, CH_3(β)]; 1.40 [12H, m, CH_2(b+c)]; 1.76 (2H,m, CH_2(2)]; 2.25 [8H, m, CH_2(a+1)]; 2.50 [2H, m, CH_2(3)]; 4.10 (2H, q, CH_2(α)]. ^{13}C NMR, δ/ppm (75,47 MHz, DMSO-d_6): 13.3 [CH_3(d)]; 14.1 [CH_3(β)]; 23.4 [CH_2(c)]; 23.7 [CH_2(b)];, 33.6, [CH_2(2)]; 58.0 [CH_2(3)]; 60.6 [CH_2(1+a)]; 62.7 [CH_2(α)]; 169.1 (C=O(4)]. ESI-MS, m/z Found (Calculated): 317.25 (317.47) [$C_{18}H_{38}PO_2^+$]; 259.24 (259.97) [$C_{11}H_{29}PO_2^+$]. IR (ν/cm^{-1}): 2960, 2928, 2874 (ν_{C-H}); 1727 ($\nu_{C=O}$); 1233 (ν_{C-N}).

The full name, abbreviation and chemical structure of the synthesized AGB-ILs are summarized in Table 2.

Table 2.

Name, abbreviation, chemical structure and molecular weight of the synthesized AGB-ILs, and of two commercial ILs investigated for comparison purposes.

Name	**Abbreviation**	**Chemical Structure and Atoms Identification**	**Molecular Weight** ($g.mol^{-1}$)
1-(4-ethoxy-4-oxobutyl)-1-methylpyrrolidin-1-ium bromide	$[MepyrNC_4]Br$	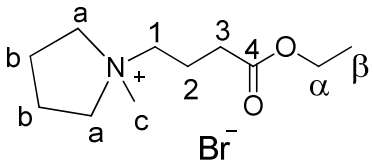	280.22
N,N,N-triethyl(4-ethoxy-4-oxobutyl)-1-aminium bromide	$[Et_3NC_4]Br$	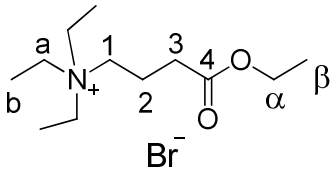	296.25
N,N,N-tri(*n*-propyl)(4-ethoxy-4-oxobutyl)-1-aminium bromide	$[Pr_3NC_4]Br$	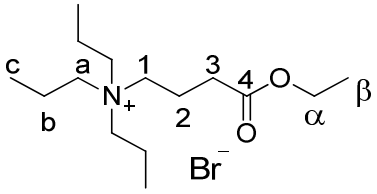	338.33
N,N,N-tri(*n*-butyl)(4-ethoxy-4-oxobutyl)-1-aminium bromide	$[Bu_3NC_4]Br$	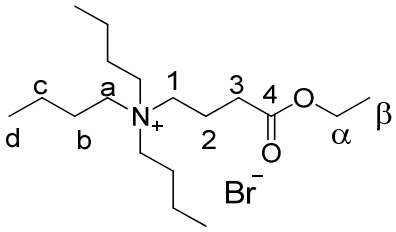	380.41
Tri(*n*-butyl)(4-ethoxy-4-oxobutyl)-1-phosphonium bromide	$[Bu_3PC_4]Br$	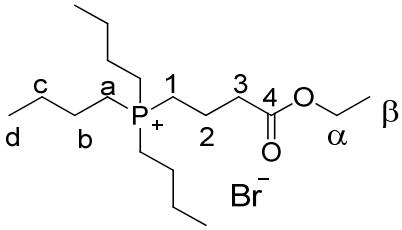	397.37
Tetra(*n*-butyl)ammonium bromide	$[N_{4444}]Br$	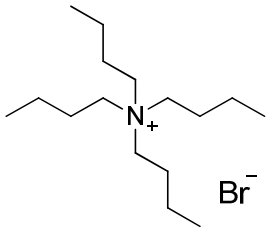	324.41
Tetra(*n*-butyl)phosphonium bromide	$[P_{4444}]Br$	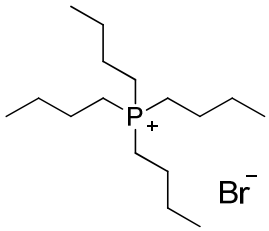	341.37

2.3. Characterization of AGB-ILs

All IL samples were dried under vacuum (10 Pa) at room temperature for a minimum of 48h before carrying out their characterization. The water content of the dried ILs was determined by Karl Fischer coulometry using a Metrohm 787 KF Titrino coulometer with Hydranal 34805 and Hydranal 37817 (from Fluka) as titrant; their water concentration was less than 6×10^{-4} in weight fraction. During the preparation of the ILs aqueous solutions for the ecotoxicity assays and ternary phase diagrams determination, the water content of each IL was taken into account. Elemental analyses (C, H, N and S contents) of all synthesized ILs were carried on a Perkin-Elmer 2400 C, H, N and S element analyzer. Infra-Red (IR) spectra were recorded at room temperature with a PerkinElmer UATR Two spectrometer. ^{1}H and ^{13}C Nuclear magnetic resonance (NMR) were recorded at room temperature with a Bruker AC 30 spectrometer (250 MHz for ^{1}H, 62.5 MHz for ^{13}C) using DMSO-d_6 as solvent. Chemical shifts (in ppm) for ^{1}H and ^{13}C NMR spectra are referenced to residual protic solvent peaks. Electrospray ionization mass spectrometry (ESI-MS) of AGB-ILs diluted in methanol were obtained on a hybrid tandem quadrupole/time-of-flight (Q-TOF) instrument, equipped with a pneumatically assisted electrospray (Z-spray) ion source (Micromass, Manchester, UK) operated in positive mode; the capillary voltage was 3500 V; and the extraction cone voltage varied between 30-60V with the flow of injection of 5 mL/min. The decomposition temperatures of the ILs were determined by thermogravimetrical analyses (TGA) using a Netzsch TG 209 F3 Tarsus thermogravimetric analyzer, under nitrogen atmosphere, with samples of 10-20 mg. These were heated from 30 °C to 500 °C, with a heating rate of 10 °C·min^{-1}. Differential Scanning Calorimetry (DSC) experiments were performed with a TA Instruments Q100, under nitrogen atmosphere, with a cooling and heating rate of 10 °C·min^{-1}.

2.4. Microtox® acute toxicity tests

To address the ecotoxicity of the synthetized AGB-ILs, the standard Microtox® liquid-phase assay [36] was used, in which it is evaluated the luminescence inhibition of the bacteria *Allvibrio fischeri* (strain NRRL B-11177) [37]. In this work, the standard 81.9% test protocol was followed [38]. The microorganism was exposed to a range of diluted aqueous solutions of each IL (from 0 to 81.9 wt%), where 100% of AGB-IL corresponds to a known concentration of a stock solution previously prepared [39]. After 5, 15 and 30 min of exposure of the bacterium to each IL aqueous solutions, the light output of the bacterium was assessed and compared with the light output of the blank control (an aqueous solution without AGB-ILs), enabling the calculation of the EC_{50} values at 5, 15 and 30 min through the Microtox® Omni™ Software [39].

2.5. ABS phase diagrams

Aqueous solutions of each IL ([MepyrNC$_4$]Br, [Et$_3$NC$_4$]Br, [Pr$_3$NC$_4$]Br, [Bu$_3$NC$_4$]Br, [Bu$_3$PC$_4$]Br) at

circa 70-90 wt% and aqueous solutions of the mixture $K_3C_6H_5O_7/C_6H_8O_7$ (as a buffer solution at pH = 7.0, mole ratio of ≈ 15:1) at ≈ 50 wt% were prepared and used for the determination of the binodal curves. The phase diagrams were determined through the cloud point titration method [40, 41] at (25 ± 1) °C and atmospheric pressure. The system compositions were determined by the weight quantification of all components added within ± 10^{-4} g. Further details on the experimental procedure can be found elsewhere [41, 42]. Tie-lines (TLs) and tie-line lengths (TLLs) were determined by a gravimetric method originally described by Merchuk et al. [43].

3. Results and discussion

3.1. AGB-ILs synthesis and characterization

Analogues of glycine-betaine ionic liquids (AGB-ILs) were obtained by the reaction of the corresponding tertiary amine and 2-bromoacetic acid ethyl ester (Figure 1). GB-ILs were obtained at yields higher than 80 %, and isolated and recovered as white solids at room temperature. ^{1}H and ^{13}C NMR spectra revealed the absence of organic impurities in the purified ILs. The electrospray ionization mass spectra of the synthesized ILs are given in Figures S1 to S5 in the Supporting Information, showing the presence of the organic cations [$MeprNC_4^+$] (m/z = 200.16), [$Et_3NC_4^+$] (m/z = 216.18), [$Pr_3NC_4^+$] (m/z = 258.24), [$Bu_3NC_4^+$] (m/z = 300.27) and [$Bu_3PC_4^+$] (m/z = 317.25).The IR spectra of all ILs show only weak absorption bands in the 3000-3100 cm^{-1} region, indicating that the interaction between the cation and anion of the ILs *via* hydrogen bonds is rather limited, a result of the bulky and organic tetraalkylammonium and phosphonium cations. Therefore, it is mainly the cation-anion coulombic attraction that ensures the cohesion of these salts. In addition, IR spectra for AGB-ILs indicate the presence of water, according to the band in the 3400 cm^{-1} region corresponding to OH stretching.

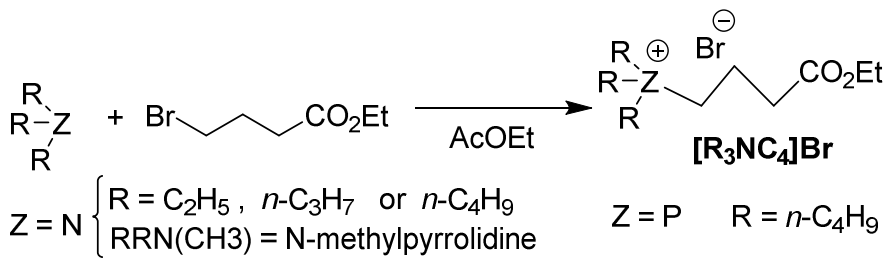

Fig. 1. Synthetic route of AGB-ILs.

The data corresponding to the AGB-ILs melting point (T_m), glass transition temperature (T_g) and decomposition temperature (T_{dec}) corresponding to 10% of weight loss are given in Table 3. Melting points were identified for all ILs, but no glass transition temperature (Tg) has been observed for [Pr_3NC_4]Br and [Bu_3PC_4]Br. The DSC results of all the synthesized salts [R_3NC_4]Br (R_3N = N-methypyrrolydinyl or R = ethyl, *n*-propyl, *n*-butyl) are given in Figure S6 in the Supporting

Information. All the synthesized ILs have melting points below 100 °C, i.e. from 73 to 90 °C , which is attributed to the bulky and asymetric cation with high charge dispersion, and thus to the poor cation-anion interactions. Furthermore, the melting points slightly increase with the alkyl chain at the cation, in agreement with the literature [44]. On the other hand, $[Bu_3PC_4]Br$ (T_m = 88 °C) shows a lower melting point than the corresponding ammonium salt $[Bu_3NC_4][Br$ (T_m = 90 °C). The same behaviour, observed with other ammonium- and phosphonium-based ILs including the commercial ones ($[N_{4444}][Br]$ with T_m = 104 °C and $[P_{4444}][Br]$ with T_m = 101 °C), was attributed to the larger radius of the phosphorus atom leading to a higher dispersion of charge [45]. It is known that the glass transition temperature is approximately two-thirds of the melting point value [46]. The range of experimental T_g/T_m ratio was found to be between 0.58 and 0.78 for different molecules and polymers [47]. The T_g/T_m of the prepared ILs (given in Table 3) ranges between 0.64 and 0.72, fitting within the range of values reported in the literature [47].

Table 3

Melting (T_m), glass transition (T_g) and decomposition (T_{dc}) temperatures for the synthesized AGB-ILs.

AGB-ILs	T_m (°C)[a]	T_g (°C)	T_g/T_m	T_{dec} (°C)
$[MepyrNC_4]Br$	73	-31	0.70	179
$[Et_3NC_4]Br$	78	-21	0.72	187
$[Pr_3NC_4]Br$	79	-	-	184
$[Bu_3NC_4]Br$	90	-40	0.64	198
$[Bu_3PC_4]Br$	88	-	-	310

(a) The uncertainty in the measured temperature was (± 0.2 °C).

The thermal stability of the synthesized AGB-ILs was determined by TGA over the temperature range between 30 and 400 °C, being the respective data given in Table 3. The thermal degradation profile of the investigated ILs is shown in Figure 2, where the decomposition temperature (T_{dec}) of all these salts falls in the range between 180 and 310 °C (Figure 2). The ILs thermal stabilities increase in the order: $[MepyrNC_4]Br$ < $[Pr_3NC_4]Br$ < $[Et_3NC_4]Br$ < $[Bu_3NC_4]Br$ << $[Bu_3PC_4]Br$. With the exception of $[Pr_3NC_4]Br$ IL (T_{dec} = 184 °C), a slight increase in the thermal stability is observed when increasing the cation alkyl chain length. addidtion, the cyclic ammonium $[MepyrNC_4]Br$ is the IL with the lowest T_{dec} confirming that the thermal stability of these ILs mostly depends on the number of carbon atoms at the cation. For the ILs comprising ammonium cations, the maximum degradation temperature is obtained with the *n*-butyl groups. Furthermore, the tri(*n*-butyl)phosphonium-based IL is more thermally stable than the respective ammonium counterpart ($[Bu_3NC_4]Br$ with T_{dec} = 198 °C *versus* $[Bu_3PC_4]Br$ with T_{dec} = 310 °C). These results are in agreement with those of other

ammonium/phosphonium-based ILs, where phosphonium-based ILs present higher values of T_{dec} [48, 49]. Tsunashima *et al.* [50] attributed this increase to the presence of empty d-orbitals on the phosphorus atom.

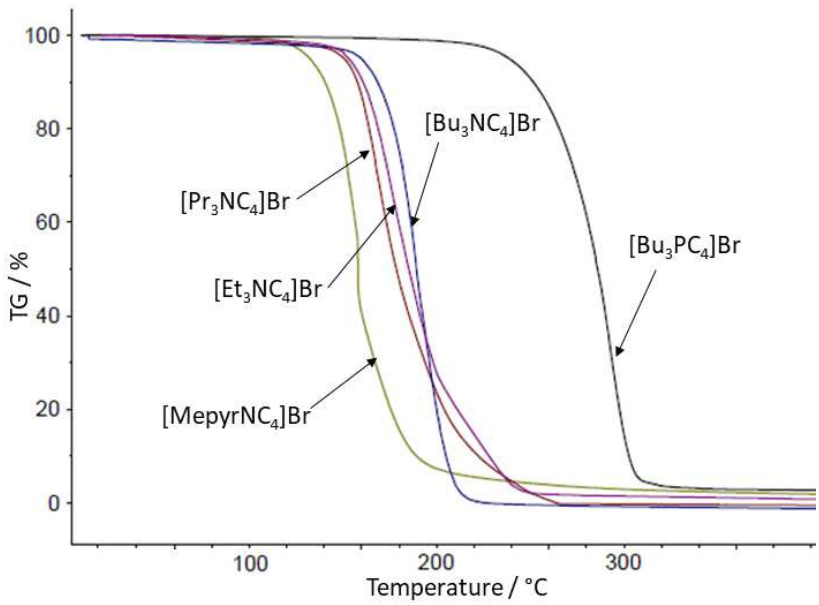

Fig. 2. TGA profiles for bromide based AGB-ILs.

The five AGB-ILs were tested in terms of their effect against the marine luminescent bacteria *Allvibrio fischeri*. The EC_{50} values determined after 5, 15 and 30 min of exposure, and the respective 95% confidence limits, are reported in Table 4. The EC_{50} data at 30 min were adopted to ensure enough exposition time to verify the full effect in the luminescence inhibition [51]. The EC_{50} values at the same times of exposure for the commercial tetrabutylammonium and tetrabutylphosphonium bromide ILs ($[N_{4444}]Br$, $[P_{4444}]Br$) [52] are also displayed in Table 4 for comparison purposes. The higher the EC_{50} values the less toxic is the IL towards this luminescent marine bacteria. Regardless of the exposure time, the results obtained show that the toxicity of AGB-ILs toward the bacteria increase according to the following sequence: $[MepyrNC_4]Br < [Et_3NC_4]Br < [Pr_3NC_4]Br < [Bu_3NC_4]Br << [Bu_3PC_4]Br$. Because all AGB-ILs share the bromide anion, the differences in their toxicity are a result of the IL cation. For the ammonium-based ILs, the toxicity increases with the alkyl chain length increase, being this a well-known trend recurrently named as the “side-chain effect” [53, 54]. The increase of the cation alkyl chain length leads to an increase of its hydrophobicity/lipophilicity, resulting in a higher ability to interact with and/or permeate phospholipid bilayers. Taking into account the cation central atom, the EC_{50} values decrease from $[Bu_3NC_4]Br$ to $[Bu_3PC_4]Br$, meaning that the ammonium-based IL is less toxic than its phosphonium-based counterpart, being in agreement with previous findings [55]. The same behavior is shown for the commercial ILs ($[N_{4444}]Br$ vs. $[P_{4444}]Br$). In general, all AGB-ILs synthesized and proposed in this work display a lower toxicity to *Allvibrio fischeri* than those

commonly used, namely [N_{4444}]Br and [P_{4444}]Br. All the studied AGB-ILs can be considered as harmless or practically harmless (at 30 min of exposure: 191 mg.L^{-1} ≤ EC_{50} ≤ 3052 mg.L^{-1}) according to Passino and Smith classification [56].

Table 4

Microtox® EC_{50} values (mg.L^{-1}) for *Allvibrio fischeri* after 5, 15 and 30 min of exposure to aqueous solutions of AGB-ILs and of two commercial ILs [51, 52] with the respective 95% confidence limits (in brackets).

AGB-ILs	EC_{50} (mg.L^{-1}) (lower limit; upper limit)		
	5 min	15 min	30 min
[$MePyrNC_4$]Br	3058.56 (1596.73; 4478.39)	3052.29 (2277.68; 4526.90)	3052.32 (1882.86; 4281.78)
[Et_3NC_4]Br	2664.15 (1917.81; 3410.5)	2491.05 (1627.56; 3354.54)	2415.00 (1621.30; 3208.70)
[Pr_3NC_4]Br	2157.05 (1678.50; 2635.61)	2026.41 (1411.48; 2641.35)	2018.72 (1267.08; 3630.37)
[Bu_3NC_4]Br	435.43 (295.60; 575.27)	380.92 (260.06; 501.78)	327.22 (317.22; 336.78)
[Bu_3PC_4]Br	351.76 (248.71; 454.83)	243.95 (239.41; 370.06)	191.30 (141.25; 200.45)
[N_{4444}]Br	233.30 (223.36; 243.15)	160.22 (143.55; 176.87)	-
[P_{4444}]Br	216.00 (21.60; 1382.40)	172.80 (0.00; 3218.40)	-

3.2. ABS phase diagrams

The novel AGB-ILs proposed in this work have low melting points, below 100 °C, display high degradation temperatures (180-310 °C), and low toxicity as shown by being harmless or practically harmless towards the marine bacteria *Allvibrio fischeri*. Therefore, their use in a wide range of applications can be envisioned. Aiming at exploring their use in liquid-liquid separation processes, we addressed here their potential to form ABS with salts. Novel ternary phase diagrams were determined for all the AGB-ILs + water + potassium citrate/citric acid mixtures ($K_3C_6H_5O_7/C_6H_8O_7$ mixtures, pH = 7.0) at 25°C and atmospheric pressure. In the respective phase diagrams, illustrated in Figure 3, the biphasic region is localized above the solubility curve described by the experimental solubility data points. Diagrams with a larger area above the binodal curve have therefore a higher ability to form two phases, i.e. the IL is more easily salted-out by the citrate-based salt [57]. For comparison purposes, the ternary phase diagrams for the commercial [N_{4444}]Br and [P_{4444}]Br under the same conditions, which were previously reported [51, 52], are also provided. The corresponding experimental weight fraction data are given in the Tables S1-S5 in the Supporting Information. All the calculations considering the

weight fraction of the phase-forming components were performed discounting the complexed water in the commercial citrate-based salt and citric acid.

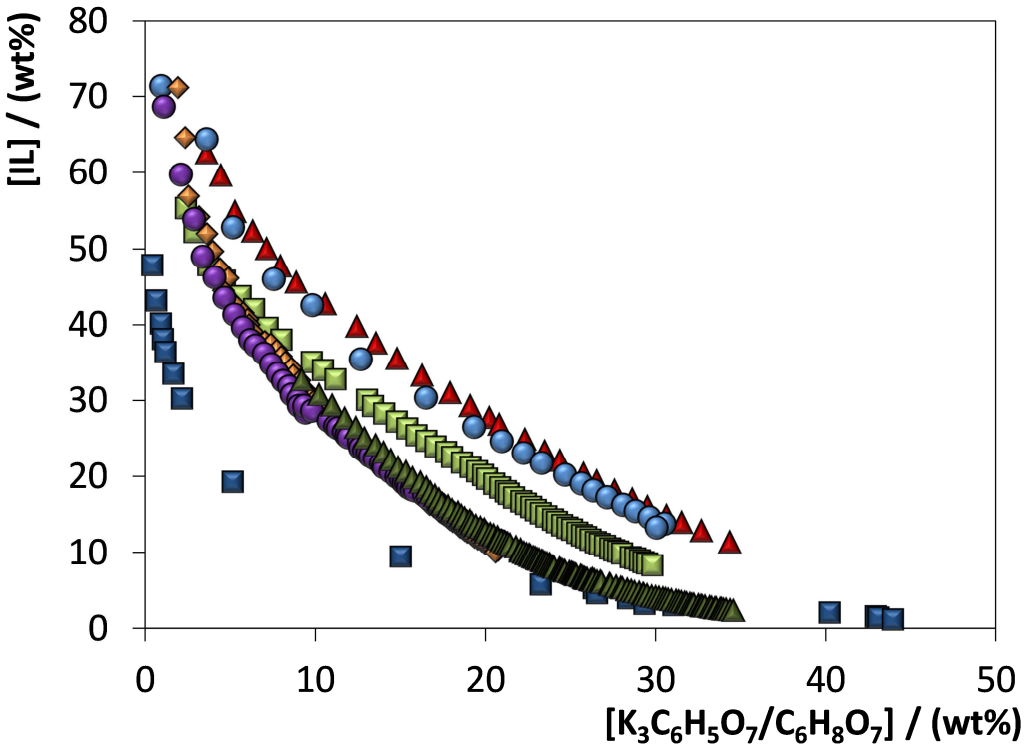

Fig. 3. Ternary phase diagrams, in an orthogonal representation, for the systems composed of IL + water + $K_3C_6H_5O_7/C_6H_8O_7$ buffered at pH = 7.0 and at 25°C: [MepyrNC$_4$]Br (▲); [Et□NC$_4$]Br (●); [Pr□NC$_4$]Br (■); [Bu□NC□]Br (◆); [Bu$_3$PC$_4$]Br (●), [N$_{4444}$]Br (▲) [57]; [P$_{4444}$]Br (■) [58].

The phase diagrams shown in Figure 3 allow the evaluation of the effect of the ammonium alkyl chain length, the effect of the IL central atom (N *vs*. P), and the presence of cyclic cation structures against linear alkyl side chains. All studied compounds comprise the bromide anion, being the difference in liquid-liquid demixing a result of the IL cation nature. The capacity of AGB-ILs to form ABS (or to be salted-out by the organic citrate-based salt) follows the order: [Bu$_3$PC$_4$]Br > [Bu$_3$NC$_4$]Br > [Pr$_3$NC$_4$]Br > [Et$_3$NC$_4$]Br ≈ [MepyrNC$_4$]Br. It is shown that the increase of the cation alkyl chain length facilitates the creation of ABS, meaning that longer alkyl side chain ILs are more easily salted-out by the organic salt, in agreement with literature data and demonstrating that this behavior is independent of the salt used [59-61]. On the other hand, [MepyrNC$_4$]Br is the IL with the lowest ability to create ABS, as result of its higher hydrophilicity afforded by a lower number of methylene groups. The phase diagrams for the systems composed of [Bu$_3$NC$_4$]Br and [Bu$_3$PC$_4$]Br are also presented in Figure 3, allowing to appraise the effect of the IL cation central atom. Although with a similar chemical structure, [Bu$_3$PC$_4$]Br presents a slightly better separation performance in presence of aqueous solutions of $K_3C_6H_5O_7/C_6H_8O_7$, in agreement with what has been previously demonstrated with other salts [62-64] and in agreement with the trend observed with the commercial ILs [P$_{4444}$]Br and [N$_{4444}$]Br. Both the

IL pairs [Bu_3PC_4]Br/[Bu_3NC_4]Br and [P_{4444}]Br/[N_{4444}]Br comprise the bromide anion, and the differences in the respective phase diagrams are a result of the charge distribution at the IL cation central heteroatom which dictates the IL affinity for water [45]. In summary, amongst the AGB-ILs investigated, [$MepyrNC_4$]Br displays the lowest capacity to create ABS and requires a higher amount of citrate-based salt to undergo phase separation, whereas [Bu_3PC_4]Br is the most effective AGB-IL and requires the lowest amount of $K_3C_6H_5O_7/C_6H_8O_7$ to form ABS. The fitting of the experimental binodal curves, and the determination of tie-line data and respective length were additionally performed, being provided in the Supporting Information (Tables S6 and S7). Even though there are 4 ions in solution, ion exchange is not expected to occur since the probability of different ion pairs to form is significantly low, as previously confirmed with ABS formed by ionic liquids and strong salting-out salts [65-66], being this the case of the current work.

In summary, it is here shown that AGB-ILs form ABS with $K_3C_6H_5O_7/C_6H_8O_7$ at controlled pH (7.0). In addition, their high thermal stability and low ecotoxicity against *Allvibrio fischeri* support their further investigation in other ABS to be applied in separation processes of labile biomolecules.

4. Conclusions

In this work, we reported the synthesis and characterization of five new water-soluble analogues of glycine-betaine-based ionic liquids (AGB-ILs) combined with the bromide anion. Their thermal properties, namely melting temperature, glass transition temperature and decomposition temperature were determined and discussed in terms of the IL chemical structure. All synthesized AGB-ILs fit within the ILs category, with a melting temperature below 100 °C, and present high degration temperatures (180-310 ºC). Their toxicity against the marine luminescent bacteria *Allvibrio fischeri* showed that the studied AGB-ILs are harmless or practically harmless and display a lower toxicity of this marine bacteria than commonly used ILs, such as [N_{4444}]Br and [P_{4444}]Br. Given the AGB-ILs properties, we studied their potential to create ABS that could be applied in separation processes. The ABS phase diagrams were determined for systems composed of AGB-IL + water + $K_3C_6H_5O_7/C_6H_8O_7$ at pH 7.0 and at 25 °C. The obtained results confirm their high ability to be salted-out by the organic salt and to form ABS, where more hydrophobic ILs more easily form two-phase systems or require a lower amount of salt to undergo phase separation in aqueous media. This ability to be salted-out by the organic salt follows the order [Bu_3PC_4]Br > [Bu_3NC_4]Br > [Pr_3NC_4]Br > [Et_3NC_4]Br ≈ [$MepyrNC_4$]Br. All the properties shown for the newly reported AGB-ILs are beneficial to develop sustainable and biocompatible separation processes.

Acknowledgments

This work was developed within the scope of the project CICECO-Aveiro Institute of Materials, FCT Ref. UID/CTM/50011/2019, financed by national funds through the FCT/MCTES. M. M. Pereira acknowledges the PhD grant (2740-13-3) and financial support from Coordenação de Aperfeiçoamento de Pessoal de Nível Superior – Capes and the Short Term Scientific Mission grant COST-STSM-ECOST-STSM-CM1206–011015-066583. M. G. Freire acknowledges the European Research Council under the European Union's Seventh Framework Programme (FP7/2007-2013)/ERC Grant 337753. We acknowledge D. Harakat for the ESI-MS measurements.

References

[1] A. Schmid, A. Koller, R.G. Mathys, B. Withot, Extremophiles 2 (1998) 249-256.

[2] T.P.T. Pham, C.W. Cho, Y.S. Yun, Water Research 44 (2010) 352-372.

[3] P. Wasserscheid and W. Keim, Angew. Chem., Int. Ed. 39 (2000) 3772-3789.

[4] M.J. Earle, K.R. Seddon, Pure Appl. Chem. 72 (2000) 1391-1398.

[5] J.L. Anderson, J. Ding, T. Welton, D.W. Armstrong, J. Am. Chem. Soc. 124 (2002) 14247-14254.

[6] J. Dupont, R.F. De Souza, P.A.Z. Suarez, Chem. Rev. 102 (2002) 3667-3692).

[7] A. Jordan, N. Gathergood, Chem. Soc. Rev., 44 (2015) ,8200-8237.

[8] D.O. Hartmann, C.S. Pereira, Toxicity of Ionic Liquids: Past, Present, and Future, Ionic Liquids in Lipid Processing and Analysis - Opportunities and Challenges, 2016, Chapter 13, Pages 403-421.]

[9] M. Amde, J.-F. Liu, L. Pang, Environ. Sci. Technol. 49 (2015) 12611−12627.

[10] S.T. Handy, Chem. Eur. J. 9 (2003) 2938-2944.

[11] D.-J. Tao, Z. Cheng, F.-F. Chen, Z.-M. Li, N. Hu, X.-S. Chen, J. Chem. Eng. Data 58 (2013), 1542−1548.

[12] N. Muhammad, M.I. Hossain, Z. Man, M. El-Harbawi, M. A. Bustam, Y. Ab. Noaman, N.B.M. Alitheen, M.K. Ng, G. Hefter, C.-Y. Yin, J. Chem. Eng. Data 57 (2012) 2191−2196.

[13] R. Vijayaraghavan, B.C. Thompson, D.R. MacFarlane, R. Kumar, M. Surianarayanan, S. Aishwarya, P.K. Sehga, Chem. Commun. 46 (2010) 294–296.

[14] Y-X. An, M.-H. Zong, H. Wu, N. Li, Bioresour. Technol. 192 (2015) 165–171.

[15] S. Yuan, Y. Chen, X. Ji, Z. Yang, X. Lu, Fluid Phase Equilib. 445 (2017) 14-24.

[16] P. Moriel, E. J. García-Suárez, M. Martínez, A. B. García, M. A. Montes-Morán, V. Calvino-Casilda, M. A. Bañares, Tetrahedron Lett. 51 (2010) 4877–4881.

[17] S. Hu, T. Jiang, Z. Zhang, A. Zhu, B. Han, J. Song, Y. Xie, W. Li , Tetrahedron Lett. 48 (2007) 5613–5617.

[18] D.-J.Tao, Z. Cheng, F.-F. Chen, Z.-M. Li, N. Hu, X.-S. Chen, J. Chem. Eng. Data 58 (2013) 58 1542−1548.

[19] X.-D. Hou, T.J. Smith, N. Li, M.-H. Zong, Biotechnol. Bioeng. 109 (2012) 2484-2493.

[20] Poletti, C. Chiappe, L. Lay, D. Pieraccini, L. Polito, G. Russo, Green Chem. 9 (2007) 337–341.

[21] A. K. Jha, N. Jain, Tetrahedron Lett. 54 (2013) 4738–4741.

[22] Y. De Gaetano, A. Mohamadou, S. Boudesocque, J. Hubert, R. Plantier-Royon, L. Dupont, J. Mol Liq. 207 (2015) 60-66.

[23] A. Messadi, A. Mohamadou, S. Boudesocque, L. Dupont, P. Fricoteaux, A. Nguyen-Van-Nhien, M. Courty, J. Mol Liq. 184 (2013) 68-72.

[24] Y. De Gaetano, J. Hubert, A. Mohamadou, S. Boudesocque, R. Plantier-Royon, J.H. Renault, L. Dupont, Chem. Eng. J. 285 (2016) 596-604.

[25] A. Messadi, A. Mohamadou, S. Boudesocque, L. Dupont, E. Guillon, Sep. Purif. Technol. 107 (2013) 172-178. 31.

[26] Y. Zhou, S.Boudesocque, A.Mohamadou, L. Dupont, Sep. Sci. Technol. 50 (2015) 38-44.

[27] S. Boudesocque, A. Mohamadou, L. Dupont, New J. Chem., 38 (2014) 5573-5581.

[28] A. M. Ferreira, E. S. Morais, A. C. Leite, A. Mohamadou, B. Holmbom, T. Holmbom, B. M. Neves, J. A. P. Coutinho, M. G. Freire, A. J. D. Silvestre, Green Chem. 19 (2017) 2626-2635.

[29] D. Coleman and N. Gathergood, Chem. Soc. Rev. 39 (2010) 600–637

[30] A. Sakamoto, N. Murata, Plant, Cell Environ. 25 (2002) 163-171.

[31] M. Ashraf, M.R. Foolad, Environ. Exp. Bot. 59 (2007) 206-216.

[32] J. R. Hoffman, N. A. Ratamess, J. Kang, S. L. Rashti and A. D. Faigenbaum, J. Int. Soc. Sports Nutr. 6 (2009) 7-7.

[33] Z. F. Nsimba, M. Paquot, L. G. Mvumbi and M. Deleu, Biotechnol. Agron. Soc. Environ. 14 (2010) 737-748.

[34] S. M. Steinberg, E. J. Poziomek, W. H. Engelmann and K. R. Rogers, Chemosphere 30 (1995) 155–2197.

[35] M. Corporation, Microtox® manual—a toxicity testing hand-book, Microbics Corporation, 1992, Carlsbad, 1–5.

[36] S.P.M. Ventura, A.M.M. Gonçalves, F. Gonçalves, J.AP. Coutinho, Aquat. Toxicol. 96 (2010) 290-297.

[37] B.T. Johnson, Microtox acute toxicty test in C. blaise J.-F. Férard (Eds), Small-scale Freshwater toxicity Investigation, Springer, Netherlands, pp. 69-105.

[38] A. Environmental, Carlbad CA, USA, 1998.

[39] Azur Environmental, 1998. Azur Environmental, Microtox Manual. www.azueenv.com.

[40] C.M.S.S. Neves, S.P.M. Ventura, M.G. Freire, I.M. Marrucho, J.A.P. Coutinho, J. Phys. Chem. B 113 (2009) 5194–5199.

[41] S.P.M. Ventura, S.G. Sousa, L.S. Serafim, Á.S. Lima, M.G. Freire, J.A.P. Coutinho, J.Chem. Eng. Data 56 (2011) 4253–4260.

[42] H. Passos, A.R. Ferreira, A.F.M. Cláudio, J.A.P. Coutinho, M.G. Freire,. Biochem. Eng. J., 67 (2012) 68-76.

[43] J.C. Merchuk, B.A. Andrews, J.A. Asenjo, J Chromatogr., B: Biomed. Sci. Appl. 711 (1998) 285-293.

[44] J. D. Holbrey and K. R. Seddon, J. Chem. Soc., Dalton Trans. (1999) 2133–2139.

[45] P.J. Carvalho, S.P.M. Ventura, M.L.S. Batista, B. Schröder, F. Gonçalves, J. Esperança, F. Mutelet, J.A.P. Coutinho J. Chem. Phys. 140 (2014) 064505.

[46] W. Kauzmann, Chem. Rev. 43 (1948) 219–256.

[47] R. G. Beauman, Polymer Sci. 9 (1952) 470–472.

[48] J. Kagimoto, K. Fukumoto, H. Ohno Chem. Commun. 2006, 2254–2256

[49] C. Maton, N. De Vos, C. V. Stevens, Chem. Soc. Rev. 42 (2013) 5963-5977.

[50] K. Tsunashima ,S. Kodama, M. Sugiya, Y. Kunugi, Electrochim. Acta 56 (2010) 762-766.

[51] S.P.M. Ventura, C.S. Marques, A.A. Rosatella, C.A.M. Alfonso, F. Gonçalves, J.P.A. Coutinho, Ecotoxicol. Environ. Saf. 76 (2012) 162-168.

[52] M. M. Pereira, J. Gomes, M. R. Almeida, J. A. P. Coutinho, A. Mohamadou, M. G. Freire, Biotechnol. Prog. **2018**, 34, 1205-1212.

[53] S. Stolte, M. Matzke, J. Arning, A. Boschen, W.R. Pitner, U. Welz-Biermann, B. Jastorff, J. Ranke, Green Chem. 9 (2007) 1170-1179

[54] S.P.M. Ventura, A.M.M. Gonçalves, T. Sintra, J. Pereira, F. Gonçalves, J.A.P. Coutinho, Ecotoxicology 22 (2013) 1-12.

[55] D.J. Couling, R.J. Bernot, K.M. Docherty, J.K. Dixon, E.J. Maginn, Green Chem. 8 (2006) 82-90.

[56] D.R.M. Passino, S.B. Smith, Environ. Toxicol. Chem. 6 (1987) 901-907.

[57] F.A. e Silva, T. Sintra, S.P.M. Ventura, J.A.P. Coutinho, Sep. Purif. Technol. 122 (2014) 315–322.

[58] M.M. Pereira, S.N. Pedro, M.V. Quentala, Á. S. Lima, J.A.P. Coutinho, M. G. Freire, J. Biotechnol. 206 (2015) 17–25.

[59] C.M.S.S. Neves, S.P.M. Ventura, M.G. Freire, I.M. Marrucho, J.A.P. Coutinho, J. Phys; Chem. B 113 (2009) 5194-5199.

[60] A.F.M. Claudio, A.M. Ferreira, S. Shahriari, M.G. Freire, J.A.P. Coutinho, J. Phys. Chem. B 115 (2011) 11145-11153.

[61] S.P.M. Ventura, S.G. Sousa, L.S. Serafim, A.S. Lima, M.G. Freire, J.A.P. Coutinho, J. Chem Eng. Data 56 (2011) 4253-4260.

[62] L.S. Louros, A.F.M. Cláudio, C.M.S.S. Neves, M. G. Freire, I.M. Marrucho, P. Jérôme, J.A.P. Coutinho, Int. J. Mol. Sci. 11 (2010) 1777-1791.

[63] M.M. Pereira, S.N. Pedro, M.V. Quental, Á.S. Lima, J.A.P. Coutinho, M .G. Freire, J. Biotechnol. 206 (2015) 17-25.

[64] T.E. Sintra, R. Cruz, S.P.M. Ventura, J.A.P. Coutinho, J. Chem. Thermodyn. 77 (2014) 206-213.

[65] C.M.S.S. Neves, M.G. Freire, J.A.P. Coutinho, RSC Adv. 2 (2012) 10882-10890.

[66] N.J. Bridges, K.E. Gutowski, R.D. Rogers, Green Chem. 9 (2007) 177-183.

Figures captions

Fig. 1. Synthetic route of AGB-ILs.

Fig. 2. TGA profile for bromide based AGB-ILs.

Fig. 3. Ternary phase diagrams, in an orthogonal representation, for the systems composed of IL + water + $K_3C_6H_5O_7/C_6H_8O_7$ buffered at pH = 7.0 and at 25°C: [MepyrNC$_4$]Br (▲); [Et□NC$_4$]Br (●); [Pr□NC$_4$]Br (■); [Bu□NC□]Br (◆); [Bu$_3$PC$_4$]Br (●), [N$_{4444}$]Br (▲) [57]; [P$_{4444}$]Br (■) [58].

496

Tables captions

Table 1

Name, CAS-number, molecular weigth, purity and suppliers of applied chemicals.

Table 2

Name, abbreviation, chemical structure and molecular weight of the synthesized AGB-ILs, and of two commercial ILs investigated for comparison purposes.

Table 3

Melting (T_m), glass transition (T_g) and decomposition (T_{dc}) temperatures for the synthesized AGB-ILs.

Table 4

Microtox® EC_{50} values ($mg.L^{-1}$) for *Allvibrio fischeri* after 5, 15 and 30 min of exposure to aqueous solutions of AGB-ILs and of two commercial ILs [51, 52] with the respective 95% confidence limits (in brackets).